2.4. Measurements of the amount of hydration water and the viscoelasticity of the polymer-hydrated layers

QCM-D is a technique used for measuring the mass of the material/molecules attached to the surface of the quartz crystal via changes in the resonant frequency, ΔF, while simultaneously obtaining information about the viscoelasticity of the layer by measuring the energy dissipation factor, D. The F-shift of the QCM-D is due to the change in the total coupled mass, including that of the water coupled to the layer. In aqueous solvents, the adsorbed film may contain a considerably large amount of water, which is sensed as a mass uptake by the QCM. By measuring the energy dissipation, it becomes possible to judge if the adsorbed film is rigid or elastic which is not possible by merely observing the frequency response. The measurements of F and D were performed with a commercial QCM-D (Q-Sense, Gothenburg, Sweden). The sensor crystals used in the measurements were 5-MHz AT-cut sputter-coated SiO_2 crystals (Q-Sense, Gothenburg, Sweden). The PMPC, PHEMA, and PMMA brush layers were prepared on the sensor crystals via the same ATRP method; [Monomer]/[Initiator] was 100/1 for all the samples. All the measurements were recorded at four different resonant frequencies (5, 15, 25, and 35 MHz). The temperature in the QCM-D liquid chamber was stabilized to 24.5 °C. Q-Sense software was used to acquire the experimental data. We measured the resonant frequencies and dissipation of both the unmodified sensor and the polymer-grafted sensor in air and water. The frequency difference measured between the unmodified sensor and the polymer-grafted sensor in air was defined as ΔF_{air}, and that in water was defined as ΔF_{water}. In a similar manner, the dissipation difference measured between the unmodified sensor and the polymer-grafted sensor in air was defined as ΔD_{air}, and that in water was defined as ΔD_{water}. $\Delta F_{water}/\Delta F_{air}$ is the hydration water ratio, which indicates the mass change due to presence of the hydration water. $\Delta D_{water}/\Delta D_{air}$ is the energy dissipation ratio, which indicates the viscoelastic change due to the hydration. The viscoelasticity of a polymer brush layer includes both the mobility of the polymer chain and fluidity of the hydration water layer.

2.5. Interfacial friction measurements

A Nanoscope IIIa AFM was used to measure the friction force. The experiments were performed in contact mode in air, water, and toluene with several times. Commercially available 200-μm-long V-shaped Si_3N_4 cantilevers (NP-S, Veeco NanoProbe Tips) with an announced force contact of 0.12 N/m were used. The surface friction force data were acquired by scanning in the Trace (T) and Retrace (R) directions with the slow scan axis disabled. The Trace/Retrace pair of scan lines provided a friction loop, and one-half of the separation between the trace and retrace frictions (TMR) was a measure of the friction force. The length of a scan was maintained at 2.0 μm and the scan rate at 2.0 Hz, yielding a sliding velocity of 8.0 μm/s. The applied load N [nN] was varied by changing the vertical deflection of the cantilever. The friction coefficient μ was calculated using Amontons' law ($F = \mu N$).

We converted the experimental normal (V_N) and lateral (V_L) deflection signals expressed in terms of voltage into normal (F_N) and lateral (F_L) forces in Newton by

$$F_N = K_N S_N V_N$$
$$F_L = K_L S_L V_L$$

where K_N and K_L are the normal and lateral force constants [N/m]; and S_N and S_L, the normal and lateral force optical deflection sensitivities [nm/V]. The abovementioned force contact of 0.12 N/m was used as the normal force contact K_N. The lateral force contact K_L was calculated by [32]

$$K_L = \frac{2K_N l^2}{3h^2(1+\upsilon)}$$

where l is the cantilever length [m]; h, the cantilever height [m]; and υ, Poisson's ratio. The S_N values can be obtained from the f–d curve in AFM; S_L is related to S_N by a relation proposed by Liu and Evans [33]. Using these factors, we could convert the voltage signals obtained from AFM into force values. The applied load was also required to be calculated. The applied load N exerted by the cantilever can be given by [34]

$$N = (D - N_0)S_N K_N$$

where D is the value of the deflection setpoint [V]; and N_0, the value of the deflection signal [V] when the cantilever is in its free state. N_0 was determined by the f–d curve measurements (Fig. 2). To obtain the values of S_N and N_0, we measured the f–d curve immediately after every friction force measurement in order to exclude the possible errors induced by the systematic drift.

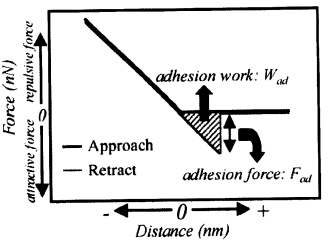

Fig. 2. Schematic illustration of the representative force–distance (f–d) curve measured by AFM and the method for defining F_{ad} and W_{ad}.

3. Results and discussion

3.1. Synthesis of the polymer brush layers via ATRP

We prepared well-controlled PMPC, PHEMA, and PMMA brush layers using ATRP. In order to control the thickness of the polymer graft layers, we controlled the polymerization degree by changing [Monomer]/[Initiator]. From ^{1}H NMR spectrum of the free polymer polymerized in an aqueous medium, we confirmed that the monomer completely converted to the desired polymer under the given conditions.

3.2. Surface characterization

The grafting of PMPC, PHEMA, and PMMA on Si wafers was confirmed using XPS (Fig. 3). The peaks in the carbon atom region (C_{1s}) at 286.5 and 289.0 eV in all the samples indicated the ether bond and ester bond in the methacrylate group, respectively. In the PMPC-grafted substrates, peaks in the nitrogen atom region (N_{1s}) at 403.0 eV attributed to the ammonium group and those in the phosphorus atom region (P_{2p}) at 133.0 eV attributed to the phosphate group were detected. These peaks were specific to the phosphorylcholine group in the PMPC unit.

The relationships of the static water contact angle and the dry thickness with [Monomer]/[Initiator] are shown in Fig. 4. The data in Fig. 4 were measured with high reproducibility and had little difference among the measured positions. The static water contact angles on the PMPC-grafted surfaces ranged from 10° to

25°. The PMPC grafting considerably increased the hydrophilicity, and a slight introduction of the PMPC chains enhanced the wettability. The contact angles on the PHEMA-grafted surfaces were approximately 40°. The hydrophilicity of the PHEMA-grafted surface was also increased. On the other hand, the contact angles on the PMMA-grafted surface were approximately 60°, similar to those on the unmodified Si. The PMMA-grafted surfaces were as hydrophobic as the unmodified Si. The thicknesses of the PMPC, PHEMA, and PMMA brush layers were 4–10, 2–7, and 2–5 nm, respectively. The thicknesses of all the polymer brushes increased with [Monomer]/[Initiator]. We prepared nanostructured polymer brush layers and controlled their thickness by changing the molar ratio of the monomer to the free initiator in the polymerization solution. The graft density σ was calculated using the dry thickness of each polymer brush layer from the equation

$$\sigma = \frac{h\rho N_A}{M_n}$$

where h is the layer thickness [nm] determined by ellipsometry; ρ, the density of each dry polymer layer (1.30 g/cm^3 for PMPC [35], 1.15 g/cm^3 for PHEMA [36], and 1.20 g/cm^3 for PMMA [37]); N_A, Avogadro's number; and M_n, the number-average molecular weight of the polymer chains on the surface. M_n was determined by measuring the molecular weight of the free polymer because these molecular weights had similar values [20]. We calculated M_n from the formula

$$M_n = \mathrm{DP} \times M_0 \times \frac{C}{100}$$

where DP is the polymerization degree determined by [Monomer]/[Initiator]; M_0, the molecular weight of each monomer; and C, the rate of conversion to the polymer determined by ^{1}H NMR measurements. The conversion rate was 100% for all the samples. The graft densities of the PMPC, PHEMA, and PMMA chains were calculated to be 0.17, 0.26, and 0.19 chains/nm^2, respectively. The graft densities of each polymer chain were relatively low compared with those in other literatures [36,37,40]. This would result from the low density of the bromoisobutyryl group at the BDCS-immobilized surface. The BDCS would not be self-assembled at the surface because it has relatively short length of the methylene chains. However, a polymer-grafted layer with a graft density of more than 0.10 chains/nm^2 forms a high-density brush structure [38,39]. It was confirmed that the polymer graft layers prepared via ATRP formed "brush" layers.

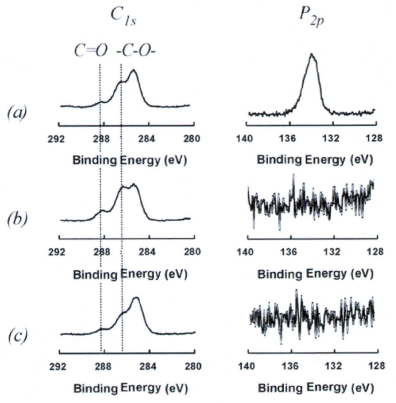

Fig. 3. The XPS spectra of (a) PMPC, (b) PHEMA, and (c) PMMA-grafted surface.

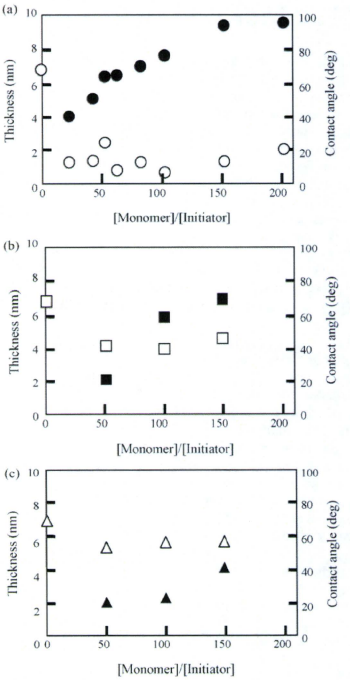

Fig. 4. Relationship between the molar ratio of the monomer to the free initiator and the static water contact angle (open plots) and the thicknesses (closed plots) of (a) the PMPC, (b) PHEMA, and (c) PMMA brush layers.

The brush conformation of the polymer graft layer examined using an AFM in air is shown in Fig. 5. Although the surface of the unmodified Si was nearly flat, the brush-like structure of each polymer graft layer was observed. The RMS surface roughness of all the samples was 0.4–0.8 nm. Compared to previous reports [40], these RMS values were very small, indicating that the polymer brush layers prepared by ATRP were considerably homogeneous with high graft densities.

3.3. Water absorptivity of the polymer brush layers and the viscoelasticity of the polymer-hydrated layers

Fig. 6 shows the hydration water ratio in each polymer brush layer, $\Delta F_{water}/\Delta F_{air}$, and the energy dissipation ratio of each polymer-hydrated layer, $\Delta D_{water}/\Delta D_{air}$. The hydration water ratio for the PMPC brush layer was the highest and decreased in the order PMPC > PHEMA > PMMA. These results indicated that most of the water molecules were coupled to the PMPC brush layer. The results of the hydration water ratio measurements accorded with those

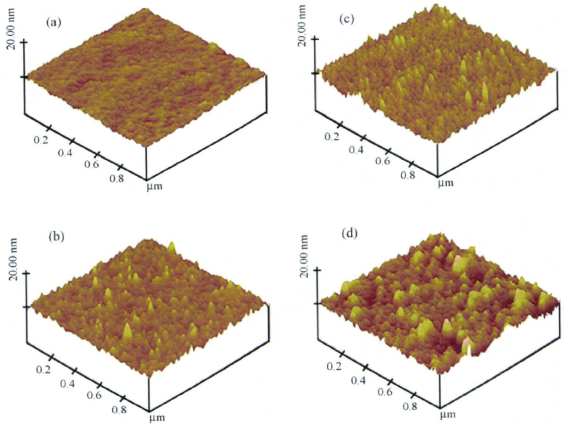

Fig. 5. AFM 3D images of (a) unmodified Si, (b) PMPC100, (c) PHEMA100, and (d) PMMA100 in air.

of the water contact angle measurements. From the values of the energy dissipation ratio, it was apparent that the PMPC-hydrated layer had the maximum fluidity in water; the PHEMA-hydrated layer had the second highest fluidity, while the PMMA-hydrated layer was the most rigid. These results indicate that the hydrophilic PMPC chains and PHEMA chains stretched in water and had greater mobility than the PMMA chains. The $\Delta D_{water}/\Delta D_{air}$ of the PMMA brush layers was negative because the PMMA chains shrink in water and the PMMA-hydrated layer is less fluid than the water layer on the unmodified SiO_2 sensor, whose surface is hydrophilic due to the presence of exposed –OH groups. Moreover, the PMPC-hydrated layer had a high energy dissipation ratio because it possessed a higher free water fraction than that of PHEMA or PMMA [19]. Generally the fluidity of free water is considerably higher than that of binding water. The results of the viscoelasticity measurements of the polymer brush layers well accorded with the previous report on the amount of free water around PMPC, PHEMA, and PMMA [19].

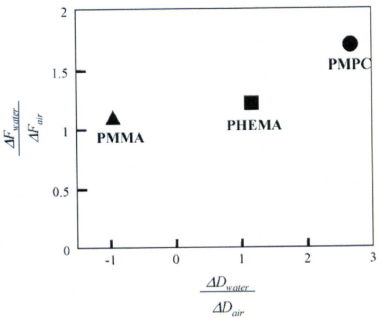

Fig. 6. The hydration water ratio in the polymer brush layer, $\Delta F_{water}/\Delta F_{air}$, and the energy dissipation ratio of the polymer-hydrated layer in water, $\Delta D_{water}/\Delta D_{air}$, measured by QCM-D.

3.4. Friction properties of the polymer brush layers and lubrication mechanism

Kobayashi and Takahara studied the lubrication of PMPC brush surface from viewpoint of macroscopic friction measurements [41]. They observed very low friction on the PMPC brush surface due to high hydrophilicity of the PMPC chains. Very recently, Klein et al. reported the lubrication of PMPC brush surface at physiological pressure and observed extremely low friction coefficient on the surface [42]. This is also due to higher hydration properties of PMPC chains. We investigated the nanoscale interfacial friction forces on the unmodified Si, PMPC, PHEMA, and PMMA brush layers using an AFM in contact mode. The representative values of the friction coefficients calculated as a function of the normal load are shown in Fig. 7. In air (Fig. 7 (a)), the friction coefficients of the PMPC brush layers were the same as those of the unmodified Si, and were characteristically high under a load less than 20 nN. When the load was above 20 nN, the friction coefficients of all the samples in air were stabilized at approximately 0.2. In contrast, in water (Fig. 7 (b)), the friction coefficients of the PMPC brush layers considerably decreased, and were below 0.08 when the load was below 20 nN. Then, the friction coefficients of the PMPC brush layers gradually increased with the normal load, and those of PMPC50, PMPC100, and PMPC150 were stabilized at approximately 0.09, 0.06, and 0.03, respectively. The friction coefficients of the PMPC brush layers in water decreased with an increase in their thicknesses of the PMPC brush layer. Fig. 7 (c) shows the friction coefficient of the PHEMA brush layers in water. When the load was below 20 nN, the friction coefficients of PHEMA50 were above 0.12, while those of PHEMA100 and PHEMA150 were below 0.12. As the normal load increased, the friction coefficients of all the PHEMA brush layers approached to approximately 0.10. Fig. 7 (d) shows the friction coefficients of the PMMA brush layers in water and those of PMMA100 in toluene. The friction coefficients of all the PMMA brush layers in water were high (above 0.2) when the

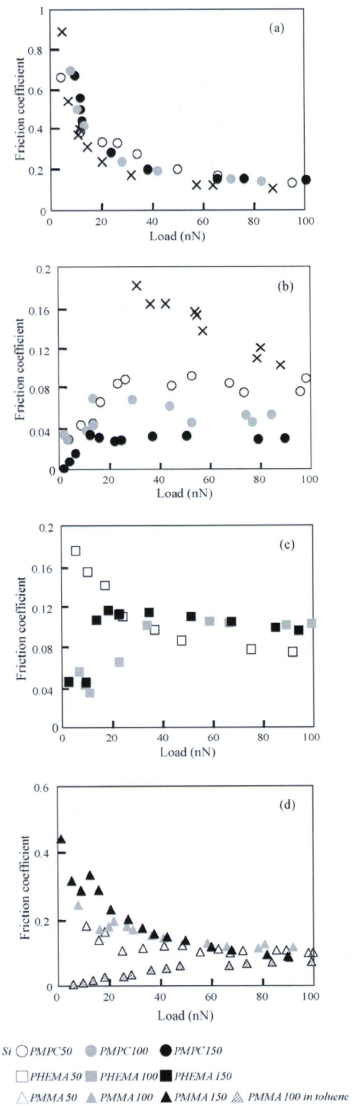

Fig. 7. The friction properties of the polymer brush layers measured by AFM: (a) the friction coefficients of the unmodified Si, PMPC50, PMPC100, and PMPC150 measured in air; (b) the friction coefficients of the unmodified Si, PMPC50, PMPC100, and PMPC150 measured in water; (c) the friction coefficients of the PHEMA50, PHEMA100, and PHEMA150 measured in water; (d) the friction coefficients of the PMMA50, PMMA100, and PMMA150 measured in water and PMMA100 measured in toluene.

load was below 20 nN. Subsequently, these values were gradually stabilized at approximately 0.15. In toluene, however, the friction coefficients of PMMA100 were clearly reduced. The friction coefficients of PMMA100 in toluene were below 0.04 when the load was below 20 nN, and gradually increased with the normal load.

The high friction coefficients for the load below 20 nN in these experiments were due to the adhesion force between the AFM cantilever and the substrate. The adhesion force between the AFM cantilever and the unmodified Si surface was 10–30 nN, as measured by the *f*–*d* curves, and acted as the load. When the load was below 20 nN, the adhesion force significantly influenced the load, thus magnifying the friction coefficients. The same adhesion force was measured on the PMPC brush layers in air. It was considered that the PMPC chains shrunk in air and were unable to prevent the interaction between the AFM cantilever and the substrate. In addition, the PMMA chains shrunk in water, and the AFM cantilever slid on the solid surface because water was a poor solvent for PMMA. The friction of the polymer brush layer only decreased when a good solvent was used for each polymer. No adhesion force between the AFM cantilever and the PMPC and PHEMA brush layers was observed in water, and a similar effect was also detected on the PMMA brush layer in toluene. In a good solvent, the polymer chains stretch and form a solvated layer that prevents the direct contact of the AFM cantilever with the substrate. Satisfying the condition of isolated friction interfaces leads to very low friction. As the normal load increased, the AFM cantilever penetrated the brush layer, and its interaction with the substrate gradually increased.

Correlating these friction properties with the results of the QCM-D measurements, it was found that both the hydration water ratio and energy dissipation ratio of the polymer-hydrated layer in water were strongly related to the friction resistance (Fig. 8). This result is consistent with the general friction theory. A usual friction phenomenon between solid surfaces is explained by the Bowden–Tabor theory [43]. In this theory, real surfaces in contact would only meet at the small areas at the peaks of their inevitable surface roughness, known as adhesion areas, where the pressure would be high and friction would be generated. In this case, friction mainly depends on the shear forces occurring at the adhesion areas, and the friction coefficient calculated by Amontons' law becomes 0.2–1.0. On the other hand, when a gas or liquid layer separates the friction interfaces and the adhesion area is absent, the friction clearly decreases. This condition is termed as hydrodynamic lubrication, and friction force F is given by [43]

$$F = \frac{\eta A v}{D}$$

where η is the viscosity of the gas or liquid layer [Ns/m^2]; A, the contact area [m^2]; v, the sliding velocity [m/s]; and D, the surface separation [m]. If the friction conditions, such as sliding size, sliding velocity, and materials used, are the same, the friction mainly depends on the surface separation distance and viscosity resistance of the layer separating the friction interfaces. The friction coefficient was dependent on the water absorptivity, because high water absorptivity led to the formation of a thick hydrated layer and large surface separation distance. Tsujii et al. have reported that the length of high-density polymer brush chains in a good solvent was approximately 2.5 times as that under dry conditions [38]. Therefore, a thick polymer brush layer could form a thick hydrated layer. This is because the friction coefficients of the PMPC and PHEMA brush layers in water depended on the thickness of

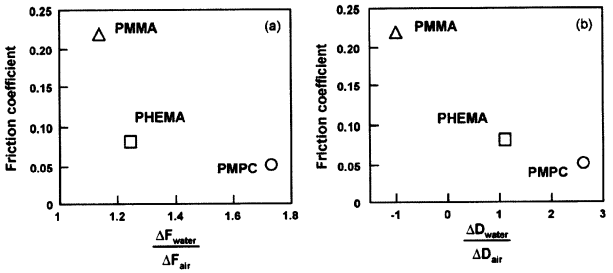

Fig. 8. Relationship (a) between the hydration water ratio, $\Delta F_{water}/\Delta F_{air}$, and the friction coefficient, and (b) between the energy dissipation ratio of the polymer-hydrated layers, $\Delta D_{water}/\Delta D_{air}$, and the friction coefficient.

the brush layers. The grafting method is significant in effecting the surface separation because a polymer layer binds to a substrate through a chemical reaction. Several previous studies have revealed that physically adsorbed polymer chains do not provide adequate wear characteristics because the physisorbed layers are observed to quickly wear away under repeated sliding cycles [44,45]. We also have reported that the polypropylene surface grafted with PMPC via a photoinduced graft polymerization method showed a good resistance against high pressure and repeated sliding cycles [46]. The dissipation ratio of the polymer-hydrated layer was related to the viscosity resistance of the layer. The high fluidity of the PMPC-hydrated layer led to low viscosity resistance. These results accorded with those mentioned in previous reports. Galliano et al. have reported lower friction coefficients for crosslinked polydimethylsiloxane (PDMS) networks with large mesh sizes; they contended that this resulted from the presence of a greater number of free and pendant chains at the interface of the large-mesh-size networks as compared to those in more tightly crosslinked networks possessing smaller mesh sizes [47]. Similar results have been reported by Gong et al. in their study of the interfacial friction of hydrogels [48,49]. They found that gels having brush-like dangling chains on their surface could manifest friction forces that were 1–2 orders of magnitude lower than those of gels without these dangling chains. These two reports indicated that the surface separation was caused by crosslinked PDMS networks or gels, and that the fluidity of the layer was caused by free and pendant chains or brush-like dangling chains.

4. Conclusions

In order to investigate the key factors responsible for the improvement of the lubricity of material surfaces, we prepared three kinds of well-controlled polymer brush layers with different monomer units and characterized them at a nanoordered level using a QCM-D and an AFM. The friction resistance was strongly correlated to the water absorptivity and fluidity of the polymer-hydrated layer. Increasing the surface separation distance with polymer-hydrated layer is the first key factor for obtaining a highly lubricated biointerface, and the high fluidity of the polymer-hydrated layer is the second key factor. PMPC grafting is a very effective and promising method for achieving both the abovementioned factors.

Acknowledgment

We thank Dr. Tomohiro Konno, the University of Tolyo and Dr. Masayuki Kyomoto, Japan Medical Materials, for providing useful discussions. Also, we are indebted to Prof. Takao Hanawa at Tokyo Medical and Dental University for ellipsometry measurements. A part of the research was supported by G-COE program "Center for Medical System Innovation".

References

[1] W.H. Harris, Clin. Orthop. 311 (1995) 46–53.
[2] A. Kobayashi, M.A. Freeman, W. Bonfield, Y. Kadoya, T. Yamac, N. Al-Saffar, G. Scott, P.A. Revell, J. Bone Joint Surg. Br. 79 (1997) 844–848.
[3] D.H. Sochart, Clin. Orthop. 363 (1999) 135–150.
[4] H. Lomas, M. Massignani, K.A. Abdullah, I. Canton, C. Lo Presti, S. MacNeil, J. Du, A. Blanazs, J. Madsen, S.P. Armes, A.L. Lewis, G. Battaglia, Faraday Discuss. 139 (2008) 143–159.
[5] K. Ishihara, M. Takai, J.R. Soc. Interf. 6 (2009) S279–S291.
[6] K. Ishihara, R. Aragaki, T. Ueda, A. Watanabe, N. Nakabayashi, J. Biomed. Mater. Res. 24 (1990) 1069–1077.
[7] K. Ishihara, N.P. Ziats, B.P. Tierney, N. Nakabayashi, J.M. Anderson, J. Biomed. Mater. Res. 25 (1991) 1397–1407.
[8] K. Ishihara, H. Oshida, Y. Endo, T. Ueda, A. Watanabe, N. Nakabayashi, J. Biomed. Mater. Res. 26 (1992) 1543–1552.
[9] S. Sawada, Y. Iwasaki, N. Nakabayashi, K. Ishihara, J. Biomed. Mater. Res. 79 (2006) 476–484.
[10] K. Sugiyama, K. Ohga, H. Aoki, Macromol. Chem. Phys. 196 (1995) 1907–1916.
[11] T. Oishi, H. Uchiyama, K. Onimura, H. Tsutsumi, Polym. J. 30 (1998) 17–22.
[12] L. Ruiz, J.G. Hilborn, D. Leonard, H.J. Mathieu, Biomaterials 19 (1998) 987–998.
[13] Y. Wang, T.J. Su, R. Green, Y. Tang, D. Styrkas, T.N. Danks, R. Bolton, J.R. Lu, Chem. Commun. (2000) 587–588.
[14] K. Ishihara, T. Ueda, N. Nakabayashi, Polym. J. 22 (1990) 355–360.
[15] K. Ishihara, H. Nomura, T. Mihara, K. Kurita, Y. Iwasaki, N. Nakabayashi, J. Biomed. Mater. Res. 39 (1998) 323–330.
[16] W. Feng, S. Zhu, K. Ishihara, J.L. Brash, Biointerphases 1 (2006) 50–60.
[17] T. Moro, Y. Takatori, K. Ishihara, T. Konno, Y. Takigawa, T. Matsushita, U. Chang, K. Nakamura, H. Kawaguchi, Nat. Mater. 3 (2004) 829–836.
[18] M. Kyomoto, T. Moro, T. Konno, H. Takadama, N. Yamasaki, H. Kawaguchi, Y. Takatori, K. Nakamura, K. Ishihara, J. Biomed. Meter. Res. Part A 82 (2007) 10–17.
[19] H. Kitano, M. Imai, T. Mori, M. Gemmei-Ide, Y. Yokoyama, K. Ishihara, Langmuir 19 (2003) 10260–10266.
[20] M. Husseman, E.E. Malmstrom, M. McNamara, M. Mate, D. Mecerreyes, D.G. Benoit, Macromolecules 32 (1999) 1424–1431.
[21] J. Pyun, T. Kowalewski, K. Matyjaszewski, Macromol. Rapid Commun. 24 (2003) 1043–1059.
[22] M.T. Muller, X. Yan, S. Lee, S.S. Perry, N.D. Spencer, Macromolecules 38 (2005) 5706–5713.
[23] A.K. Dutta, G. Belfort, Langmuir 23 (2007) 3088–3094.
[24] R. Kaneko, Tribol. Int. 28 (1995) 195.
[25] B. Bhushan, Proc. Inst. Mech. Eng. Part J 212 (1998) 1.
[26] J. Hu, X. Xiao, D.F. Ogletree, M. Salmeron, Surf. Sci. 327 (1995) 358.
[27] S.W. Zhang, H.Q. Lan, Tribol. Int. 35 (2002) 321.
[28] Q. Zhang, L.A. Archer, Langmuir 23 (2005) 7562–7570.
[29] A. Ramakrishnan, R. Dhamodharan, J. Ruhe, Macromol. Rapid Commun. 23 (2002) 612–616.
[30] I.Y. Ma, J. Lobb, N.C. Billingham, S.P. Armes, A.L. Lewis, A.W. Lloyd, J. Salvage, Macromolecules 35 (2002) 9306–9314.
[31] S. Hu, Y. Wang, K. McGinty, W.J. Brittain, Eur. Polym. J. 42 (2006) 2053–2058.
[32] E. Tocha, H. Schonherr, G.J. Vancso, Langmuir 22 (2006) 2340–2350.
[33] Y. Liu, D.F. Evans, Langmuir 12 (1996) 1235–1244.
[34] J. Li, C. Wang, G. Shang, Q. Xu, Z. Lin, J. Guan, C. Bai, Langmuir 15 (1999) 7662–7669.

[35] R. Iwata, P. Suk-In, V.P. Hoven, A. Takahara, K. Akiyoshi, Y. Iwasaki, Biomacromolecules 5 (2004) 2308–2314.
[36] C. Yoshikawa, A. Goto, Y. Tsujii, T. Fukuda, T. Kimura, K. Yamamoto, A. Kishida, Macromolecules 39 (2006) 2284–2290.
[37] B. Chao, Langmuir 20 (2004) 11748–11755.
[38] Y. Tsujii, K. Ohno, S. Yamamoto, A. Goto, T. Fukuda, Adv. Polym. Sci. 197 (2006) 1–45.
[39] T. Wu, K. Efimenko, J. Genzer, J. Am. Chem. Soc. 124 (2002) 9394–9395.
[40] W. Feng, J.L. Brash, S. Zhu, Biomaterials 27 (2006) 847–855.
[41] M. Kobayashi, Y. Terayama, N. Hosaka, M. Kaido, A. Suzuki, N. Yamada, N. Torikai, K. Ishihara, A. Takahara, Soft Mater. 3 (2007) 740–746.
[42] M. Chen, W.H. Briscoe, S.P. Armes, J. Klein, Science 323 (2009) 1698–1701.
[43] D.F. Moore, Principle and Application of Tribology, Pergamon Press, Oxford, 1975.
[44] V.V. Tsukruk, Adv. Mater. 13 (2001) 95–108.
[45] T. Bouhacina, J.P. Aime, D. Gauthier, V. Michel, V. Heroguez, Phys. Rev. B 56 (1997) 7694–7703.
[46] K. Kitano, R. Matsuno, T. Konno, M. Takai, K. Ishihara, Trans. Mater. Res. Soc. Japan 32 (2007) 579–582.
[47] A. Galliano, S. Bistac, J.J. Schultz, Colloid Interf. Sci. 265 (2003) 372–379.
[48] J.P. Gong, T. Kurokawa, T. Narita, G. Kagata, Y. Osada, G. Nishimura, M. Kinjo, J. Am. Chem. Soc. 123 (2001) 5582–5583.
[49] T. Tada, D. Kaneko, J.P. Gong, T. Kaneko, Y. Osada, Tribol. Lett. 17 (2004) 505–511.

ORIGINAL ARTICLE

Effect of Lubricant on Wear Behavior of Ultrahigh-molecular-weight Polyethylene Cups Against Zirconia Head in Hip Joint Simulator

Masami HASHIMOTO[1], Mineo MIZUNO[1], Satoshi KITAOKA[1], Hiroaki TAKADAMA[2], and Masaru UENO[3]

[1] *Japan Fine Ceramics Center, Nagoya, Japan*
[2] *Chubu University, Nagoya, Japan*
[3] *Japan Medical Materials Corporation, Osaka, Japan*

Synopsis

The wear behavior of a femoral head made of zirconia (ZrO_2) against an acetabular cup made of ultrahigh-molecular-weight polyethylene (UHMWPE) was investigated using a hip joint simulator for five types of lubricants. Five types of lubricants were used: balanced salt solution (BSS), a BSS solution containing bovine serum albumin (A) and γ-globulin (G) (BSS+A+G), and a BSS solution containing 1.5 times the concentrations of A and G (BSS+1.5(A+G)), as well as two types of bovine sera (CS1 and CS2). The effect of the total protein concentration in the lubricant on the wear rate was assessed. The weight loss of the UHMWPE cup was measured. Weight loss increased with the test duration for all lubricants except for BSS. The lubricant that produced the highest wear rate ($mg/10^6$ cycles) calculated from the weight loss during the test, was BSS+1.5(A+G), followed by BSS+A+G. Little weight change of the UHMWPE cup was observed for BSS. The wear rate increased with the concentration of protein, irrespective of the protein species. During the experimental observation period, the wear rate decreased in the order CS1 > BSS+1.5(A+G) > CS2 > BSS+A+G > BSS $\simeq$ 0. The comparison of quantitative measurements of individual particles in the lubricants showed that the morphology of each type of particle was dependent on the type of lubricant. Fibers and/or granules appeared in CS1 and CS2. In contrast, elongated fibers were mainly generated in BSS+A+G and BSS+1.5(A+G). These elongated particles formed by wear suggest that an adhesive mechanism, rather than the abrasive mechanism associated with asperities, was active. Our results suggest that the adhesive mechanism was active in lubricants containing proteins such as A and G.

Key words: *hip joint, wear, hip simulator, lubricant, polyethylene debris*

Introduction

The ultimate goal in the design of a hip joint wear simulator and the associated test protocol is to reproduce the type and amount of wear that occur clinically. Commonly used hip simulators vary markedly in load and motion characteristics [1–3], and use various lubricants, including distilled water, physiological saline, blood serum, synovial fluid, mineral oil and synthetic serum. Comparative studies have shown that the type and amount of wear that occur in physiological lubricants (i.e., serum and synovial fluid) more

closely resemble those occurring *in vivo*, probably partly due to boundary lubrication by proteins [4–7]. It has also been shown that the type and amount of wear vary with the type of protein present in the lubricant and the concentration of the protein [8, 9].

At present, the international standard recommends calf or bovine serum that is pure or diluted with distilled water as the best substitute for synovial fluid in *in vitro* tests, but there is not complete agreement concerning this choice. In fact, the protein concentration of various commercially available serum products varies over a wide range (40-80 mg/ml) and the protein concentration of lubricants has a marked effect on the friction and wear of tribological pairs used in prosthetic joints. It is not easy to achieve reproducible results or to compare the results obtained by different laboratories. Therefore, it is desirable to develop, as an alternative to bovine serum, a stable and reliable lubricant whose composition can always be set to a specified value at the beginning of a wear test.

We previously prepared several lubricant solutions composed one or more of the major components in bovine serum, such as bovine serum albumin (A), γ-globulin (G) and a lipid with some additives [10]. The change in weight of the ultrahigh-molecular-weight polyethylene (UHMWPE) cups was dependent on the component. In the case of a one-component lubricant solution, the weight change revealed that the G solution produced the largest wear rate, but lecithin solution produced a lower wear rate than bovine serum. The weight change in two-component solutions containing A and G was similar to that in bovine serum. Moreover, the two-component solution containing A and G was stable. Therefore, this solution may serve as a particularly good model solution for the study of the wear properties of the hip joint. Owing to the importance of the particle characteristics in the quantity and quality of biological responses, great emphasis has been placed on developing techniques for extracting and studying the quantity, size and morphology of UHMWPE wear particles [11, 12].

In this study, we investigated the wear behavior of a zirconia (ZrO_2)/UHMWPE coupling in a two-component solution containing A and G using a hip joint simulator. The effect of the type of lubricant on the wear properties and the morphology of the wear debris was also investigated.

Materials and Methods

1. Materials and hip simulator

The wear behavior of a ZrO_2/UHMWPE coupling was investigated using a hip joint simulator. A ZrO_2 femoral head component with a diameter of 26 mm (Japan Medical Materials Corp., Osaka, Japan) was used. The ZrO_2 was 3 mol% yttria - doped tetragonal zirconia polycrystalline (3Y-TZP). The UHMWPE acetabular cup used was a commercially available component used in surgical implants (Japan Medical Materials Corp.). The inner and outer diameters of the UHMWPE cup were 26 and 50 mm, respectively. Two couplings were prepared for each condition.

A 12-station hip joint simulator (MTS Systems Corp., MN, USA) was used in the wear test. In the simulator, the acetabular cup was mounted above the femoral head in an upright position (Fig. 1). Motion was imparted to the femoral head through an inclined rotating bearing block. This produced a cross-path pattern at all fixed points on the articular interface. A physiological

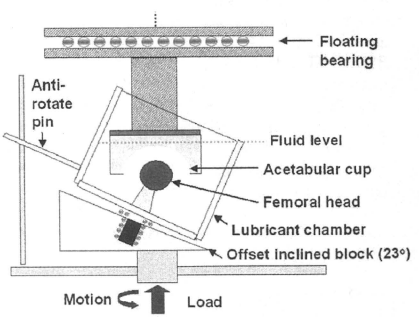

Figure 1 Schematic diagram of the MTS hip joint simulator.

cyclic load was applied to the acetabular cup via a hydraulic acutuator mounted below the inclined block. Loads simulating a physiological loading curve with double peaks of 1.8 and 2.8 kN were applied. Loading and motion were synchronized at 1 Hz. Both the head and cup were completely immersed in 750 ml of fluid. The compositions of the prepared artificial lubricants are listed in Table 1. They were prepared by dissolving reagent-grade A and G (Nacalai Tesque, Inc., Kyoto, Japan) into a phosphate buffered saline with tri-sodium hydrogen ethylene diaminetetraacetate (3Na-EDTA) (Nacalai Tesque, Inc.) and sodium azide (NaN_3) (Wako Ltd., Osaka, Japan). 3Na-EDTA and NaN_3 were added to stabilize the proteins in the solution and to keep the pH close to that in the body. The concentrations of NaCl, Na_2HPO_4, 3Na-EDTA and NaN_3 were set at 0.8%, 10 mM, 20 mM and 0.1%, respectively. The concentration of each protein in the solutions except BSS+1.5(A+G) was set at 25% of that of human serum in accordance with ISO 14242-1, while the concentration of BSS+1.5(A+G) was set at 1.5 times of that of BSS+A+G solution. As a reference, the base lubricants used were phosphate buffered saline and calf sera from two companies: Sigma-Aldrich Japan (Tokyo, Japan) (CS1) and BioWest (Nuaill, France) (CS2) (Table 1). A mixture of 25 vol% bovine serum, 20 mmol/L of ethylene diamine tetraacetic acid (EDTA), and 0.1 mass% sodium azide was used as a lubricant, in accordance with the ISO-14242-1 standard. Testing was performed until 5.0 x 10^6 cycles were completed.

2. Wear characterization

All the lubricants were changed after every 0.5 x 10^6 cycles during the tests. When the lubricant was changed, all the cups were cleaned, dried and weighed using an electronic balance (resolution: 0.01 mg) to determine the weight loss. The cups were washed using a four-step procedure. First, the cups were cleaned in an ultrasonic bath for 10 min with a soap-water solution. Second, the cups were ultrasonically cleaned in deionized water for 10 min. Third, the cups were ultrasonically cleaned in ethanol for 10 min. Lastly, the cups were vacuum-dried for 30 min to remove excess water from the surface. The net weight losses for each cup were plotted against the number of test cycles.

3. Debris extraction and SEM

A sample of each lubricant used in the test was obtained when the simulators were stopped for the gravimetric analysis of wear performance. From the 750 ml lubricant bath, 10 ml was taken during digestion and debris extraction. The homogeneity of the lubricant was ensured by agitating it prior to sampling. In each case, synovial fluid was digested using the same amount of 10 M sodium hydroxide at 65 °C for 3 h, added to a sucrose (1.2 g/ml) and isopropyl alcohol (0.919 g/ml) solution with a density gradient in a 30 ml tube, and ultracentrifuged at 114,500 g at 4 °C for 3 h (Hitachi Koki Co, Ltd., Tokyo, Japan). The interface layer was collected and mixed with methyl alcohol in another 30 ml tube, and ultracentrifuged again at 114,500 g for 3 h. The bottom layer was added to sucrose (1.05 g/ml)

Table 1 Concentrations of solutions in lubricants used in wear tests.

Lubricant (mg/ml)	NaCl	$Na_2HPO_4 \cdot 12H_2O$	Protein (Total)	Albumin	Globulin		
					α-G	β-G	γ-G
BSS	8	3.58	0	0	0	0	0
BSS+A+G	8	3.58	10.7	7.3	0	0	3.4
BSS+1.5(A+G)	8	3.58	16.2	11.1	0	0	5.1
CS1	*1	0	18.3	8.4	2.7	3.4	3.8
CS2	*2	0	15.5	7.8	2.3	4.0	1.4

*1 Na 3.38 mg/ml, *2 Na 3.24 mg/ml

and isopropyl alcohol solution (0.973 and 0.919 g/ml) with a density gradient and ultra-centrifuged again at 114,500 g for 3 h. UHMWPE debris was collected from the interface between the two layers and filtered through a 0.1 μm filter. The UHMWPE debris was examined using a JSM-633OF FE-SEM system (JEOL DATUM Co., Ltd., Nagoya, Japan) after coating it with a thin Au film.

4. Debris analysis

Digital images of individual UHMWPE debris particles were extracted from archival scanning electron micrographs. UHMWPE debris analysis was conducted by computer using a customized application based on public-domain image-processing (3D Volume, RATOC System, Tokyo, Japan) and analysis programs (Image J, National Institute of Health, Maryland, U.S.A.). UHMWPE debris particles were outlined by binary image processing and analyzed to obtain six shape and size parameters for each particle: number, area (S), particle size (PS), equivalent circle diameter (ECD), aspect ratio (AR) and circularity (R). PS is the major diameter of the particle. ECD is a measure of the size, defined as the diameter of the circle with an area equivalent to the area of the particle, and has a unit of length. Thus, the area (S) of the particle is first determined using image analysis then ECD is calculated using

$$ECD=2(S/\pi)^{1/2}. \quad (1)$$

AR is the ratio of the minor diameter to the major diameter. R is a measure of how closely the particle resembles a circle, with a perfect circle having a value of 1. The distributions of the four shape and size parameters (PS, ECD, AR and R) were plotted. The mean values of these four shape and size parameters were also derived.

Results

Figure 2 shows a plot of the cumulative weight loss of the UHMWPE cups as a function of test duration for the five lubricants. With the exception BSS, the weight loss of the cups increased with test duration. The total amounts of weight loss for BSS+A+G and BSS+1.5(A+G) after 5.0 x 10^6 cycles were 61.3 and 87.2 mg, respectively. In the cases of the sera, the total weight loss for CS1 after 5.0 x 10^6 cycles was 210.3 mg. In contrast, UHMWPE subjected to CS2 had a lower average wear rate throughout the test. After 5.0 x 10^6 cycles in CS2, the total weight loss of UHMWPE was 64.6 mg. We defined the initial wear rate as that from the first cycle up to the 1.0 x 10^6 th cycle and the steady wear rate as that from the 4.0 x 10^6 th cycle to the 5.0 x 10^6 th cycle. The following initial and steady wear rates were obtained: 13.1 and 15.7 mg / 10^6 cycles for BSS+A+G, 15.1 and 20.7 mg / 10^6 cycles for BSS+1.5(A+G), 27.9 and 47.3 mg / 10^6 cycles for CS1, and 16.9 and 13.7 mg / 10^6 cycles for CS2, respectively. These results revealed that BSS+1.5(A+G) exhibits relatively similar wear rates to bovine serum.

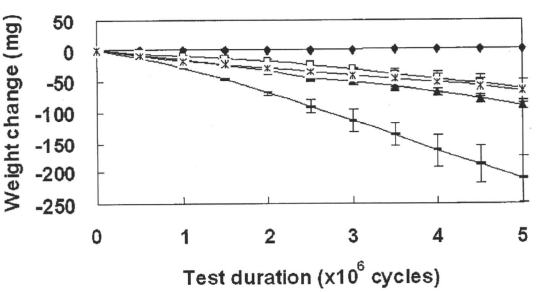

Figure 2 Plot of cumulative weight loss of UHMWPE cups as a function of test duration for various lubricants: BSS (◆), BSS+A+G (□), BSS+1.5(A+G) (▲), CS1 (-) and CS2 (*).

Figure 3 shows SEM images of UHMWPE debris isolated from the various lubricants after 5.0 x 10^6 cycles. No debris was observed in BSS (Fig. 3(a)). Elongated fibers were observed in BSS+A+G and BSS+1.5(A+G) (Figs. 3(b) and (c), respectively). Fibers and / or granules were observed in CS1 and CS2 (Figs. 3(d) and (e), respectively).

Table 2 shows the number and area of UHMWPE debris particles generated in the lubricants. The number and area of particles were significantly different among the lubricants. The number and area showed that particles generated in BSS tended to be most low value and those generated in CS1 were most high value, with intermediate values for the particles generated in

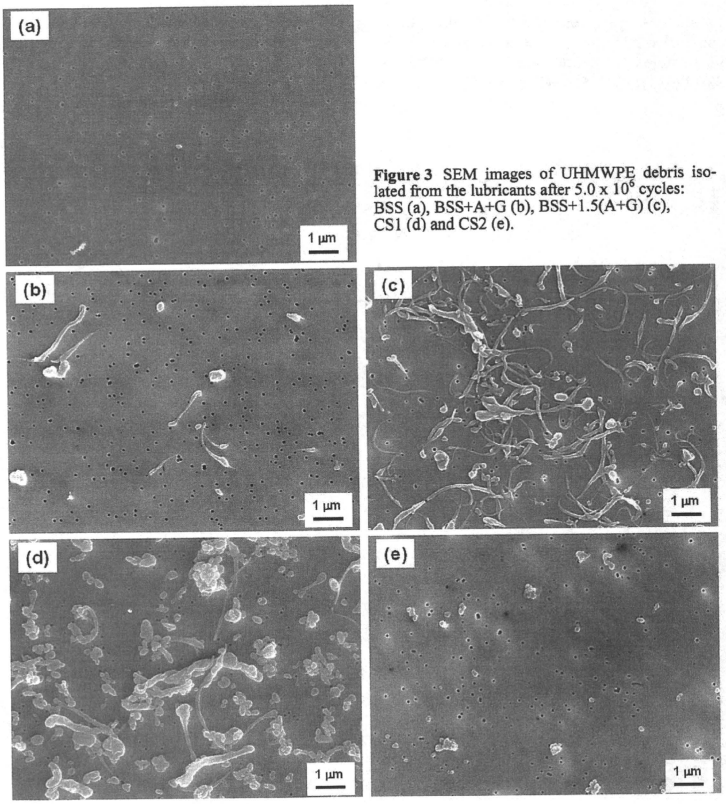

Figure 3 SEM images of UHMWPE debris isolated from the lubricants after 5.0 x 10^6 cycles: BSS (a), BSS+A+G (b), BSS+1.5(A+G) (c), CS1 (d) and CS2 (e).

BSS+A+G, BSS+1.5(A+G) and CS2. These results are consistent with the weight changes of the UHMWPE cups (Fig. 2).

The results of quantitative analysis of the UHMWPE wear debris generated in the lubricants are presented in Table 3 in the form of mean value ± standard error. The mean values of PS, ECD, AR and R were significantly different among the lubricants. It is apparent that the largest particles (mean PS: 0.89±1.40, mean ECD: 0.50±0.61) tended to be generated in CS1. The smallest particles (mean PS: 0.29±0.17, mean ECD: 0.16±0.07) were generated in BSS, with particles of intermediate sizes generated in BSS+A+G, BSS+1.5(A+G) and CS2. As might be expected, the values of mean AR indicate that elongated particles tended to be generated in BSS+A+G and BSS+1.5(A+G) (mean AR: 4.53±4.26 (BSS+A+G), 4.74±3.34 (BSS+1.5(A+G)). Particles generated in BSS, CS1 and CS2 tended to have lower ARs than those in BSS+A+G and BSS+1.5(A+G). The analysis of values of R showed that particles generated in BSS tended to be the most circular (mean R: 0.83±0.27) and those generated in BSS+1.5(A+G) were the least circular (mean R: 0.49±0.33), with intermediate values for the particles generated in BSS+A+G, CS1 and CS2 (mean R: 0.63±0.34 (BSS+A+G), 0.70±0.29 (CS1), 0.66±0.24 (CS2)).

Table 2 Number and area of UHMWPE wear debris particles generated in various lubricants.

Lubricant	Number / ml	Area / (μm^2 / ml)
BSS	1	0.02
BSS+A+G	17	2.06
BSS+1.5(A+G)	178	33.9
CS1	362	175.6
CS2	77	16.6

Table 3 Results of quantitative analysis of UHMWPE wear debris generated in various lubricants.

Lubricant	Particle size / μm	ECD / μm	Aspect ratio	Circularity
BSS	0.29±0.17	0.16±0.07	2.89±1.49	0.83±0.27
BSS+A+G	0.68±0.83	0.28±0.27	4.53±4.26	0.63±0.34
BSS+1.5(A+G)	0.81±1.00	0.35±0.35	4.74±3.34	0.49±0.33
CS1	0.89±1.40	0.50±0.61	2.76±1.73	0.70±0.29
CS2	0.52±0.65	0.31±0.31	2.71±1.08	0.66±0.24

All values expressed as mean±standard error.

Figure 4 shows the particle size distribution in the 0 – 20μm range for wear debris particles isolated from the lubricants. The distribution shows that the majority of particles removed from the surface were of 1 μm order in size. However, the particles isolated from CS1 and CS2 had a larger modal size than particles from BSS+A+G and BSS+1.5(A+G). For example, all of the particles isolated from BSS+A+G and BSS+1.5(A+G) were in the 0.5 – 5 μm size range, whereas those isolated from CS1 and CS2 were in the 0.5 – 17.5 μm size range.

Figure 5 shows the ECD distribution in the 0.5 – 7.5 μm range for the wear debris particles isolated from the lubricants. The distribution shows that the majority of particles removed from the surface had an ECD of less than 1 μm. However, the debris particles isolated from CS1 and CS2 had a considerably larger modal volume of ECD than that of particles from BSS+A+G and BSS+1.5(A+G). For instance, the ECD of particles isolated from BSS+A+G and BSS+1.5(A+G) was in the 0.5 – 2 μm range, whereas the ECD of particles isolated from CS1

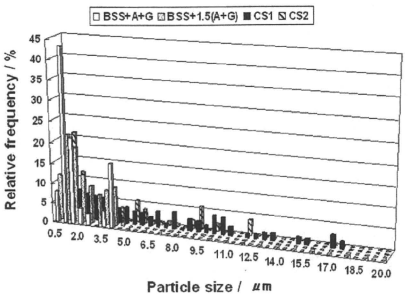

Figure 4 Frequency distribution of size of UHMWPE debris particles isolated from various lubricants.

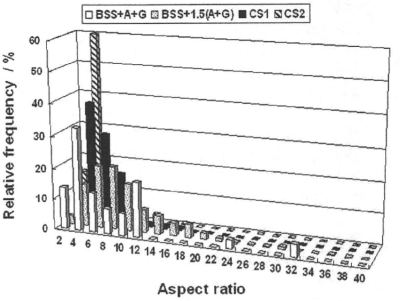

Figure 6 Frequency distribution of aspect ratio of UHMWPE debris particles isolated from various lubricants.

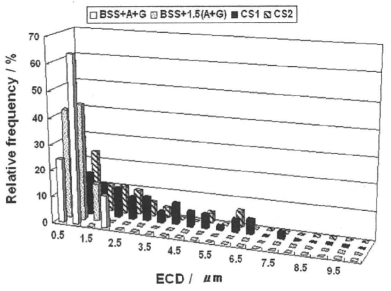

Figure 5 Frequency distribution of ECD of UHMWPE debris particles isolated from various lubricants.

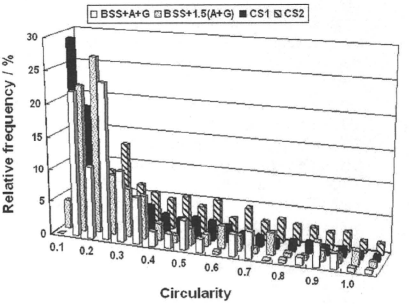

Figure 7 Frequency distribution of circularity of UHMWPE debris particles isolated from various lubricants.

and CS2 was in the 0.5 – 7.5 μm range. The type of lubricant appeared to affect the particle size and ECD.

Figure 6 shows the aspect ratio distribution for the wear debris particles isolated from the lubricants. The distribution shows that the majority of particles removed from the surface had an aspect ratio of 4. The debris particles isolated from BSS+A+G and BSS+1.5(A+G) tended to have a higher aspect ratio than those isolated from CS1 and CS2. For instance, the aspect ratios of particles isolated from BSS+A+G and BSS+1.5(A+G) were in the 2 – 32 range, whereas those of particles isolated from CS1 and CS2 were in the 2 – 16 range.

Figure 7 shows the distribution of circularity for the wear debris particles isolated from the lubricants. The most frequently occurring value of circularity was within 0.1 – 0.2. About 80% of the particles isolated from BSS+1.5(A+G) had a circularity of 0.1 – 0.5, whereas those isolated from BSS+1.5(A+G), CS1 and CS2 mostly had a circularity of 0.1 – 0.4.

Discussion

In this study, a hip wear simulator was used to evaluate the wear of UHMWPE cups in various lubricants. Gravimetric wear rates and the quantitative measurements of wear debris were used in the evaluation. As expected, the weight loss due to the wear of the UHMWPE inserts increased with the number of test cycles, but the wear rate remained constant after a certain number of cycles, suggesting that a steady-state wear regime had been attained. However, the wear rate mainly depended on the total concentration of protein, irrespective of the type of lubricant (Fig. 2). The lubricant that produced the highest wear rate was BSS+1.5(A+G), which produced almost the same wear rate as CS1 up to the 1.0×10^6 th cycle, followed by BSS+A+G. Compared with these protein-containing lubricants, the protein-free lubricant (BSS) has very low friction. The wear rate from the first cycle up to the 1.0×10^6 th cycle (initial wear rate) remained relatively low but started to increase from the 4.0×10^6 th to 5.0×10^6 th cycle (steady wear rate).

The adsorption of albumin on prosthetic materials during contact with protein-containing solutions has been reported by several authors [13–15]. This albumin layer protects the surface of metals, zirconia and UHMWPE leading to the reduction of the friction coefficient to a low value. However, the albumin did not protect the surfaces of the alumina/UHMWPE coupling [16]. Norde *et al.* reported that the main components of the intermolecular forces responsible for protein adsorption are hydrophobic and electrostatic interactions [17]. In general, most proteins tend to be adsorbed more strongly on hydrophobic surfaces [18]. Furthermore, the adsorption of proteins that are able to undergo large conformational changes, the so-called soft proteins, is not generally dictated by electrostatic interactions [19]. The metal and zirconia have more hydrophobic surface than alumina. Also, in a simulation using a ZrO_2 head and a UHMWPE cup in bovine serum, the mean temperature increased to over 55 °C without forced cooling [20]. It is considered that the adsorbed albumin underwent large conformational changes under these conditions. Therefore, the adsorption of albumin protects the surfaces of the ZrO_2/UHMWPE hip joint.

In our studies, the ZrO_2/UHMWPE coupling was used in the hip simulator. The wear rate of UHMWPE against zirconia in this experiment increased, which was the same as that of UHMWPE against alumina. This was closely related to the experimental condition of hip simulator, as was observed *in vivo*. In fact, head and cup were completely immersed in a large amount of fluid (750 ml). On the other hand, temperature of this fluid was not controlled. These suggest that the presence of albumin in the lubricant did not avoid the adhesion and transfer of UHMWPE surface in our experiment.

The UHMWPE cup in CS1 exhibited a large weight loss throughout the wear testing, suggesting that it had been scored by third-body debris, possibly denatured protein particles from the serum. During the testing, particulates were precipitated in CS2. It is considered that the high protein concentration causes the proteins present in the lubricant to degrade and subsequently form proteinaceous precipitates. These precipitates cause an increase in UHMWPE wear and scratch the ZrO_2 counterface if they become trapped in the articulation.

The UHMWPE micron- and submicron-sized debris particles exhibited an inhomogeneous morphology that was consistent with previously proposed wear mechanisms. The determination of the wear mechanism from the particle morphology is complicated. Several primary wear mechanisms for hip cups have been proposed, including microasperity wear [21–24], microadhesive wear [21,

23] and residual subsurface strain [25, 26]. Fatigue and third-body wear may also be important secondary or tertiary mechanisms and may be responsible for the production of the larger particles.

Especially, two primary damage mechanisms, namely adhesive and abrasive wear, are commonly observed in surgically explanted UHMWPE components. Adhesive wear generally follows the orientation and strain hardening of the implant surface and subsequent implant motion results in the removal of small elongated wear particles, usually on the order of a few micrometers or less in size. Abrasive wear occurs through the rubbing action of the hard asperities on the surface of the femoral component. It is also accentuated by hard third body particles, such as bone chips or bone cement particles, within the articulation. Abrasive wear progresses by the cutting and removal of the polyethylene articular surface.

The appearance of elongated wear particles suggests that an adhesive mechanism, rather than the abrasive mechanism associated with asperities, was active [27]. The small submicron-sized granules may be the result of the comminution of the fibrils or may be an ultrastructural feature of the polymer [28]. In our studies, elongated wear particles with larger values of AR and smaller values of R were generated in BSS+A+G and BSS+1.5(A+G) (Table 3). The wear debris particles corresponding to BSS+A+G and BSS+1.5(A+G) were mainly of submicron size: 60% of the analyzed particles were in the 0.5 – 1.0 μm size ranges. Our results indicate that an adhesive wear mechanism occurred in BSS+A+G and BSS+1.5(A+G).

In conclusion, the results of our study suggest that the wear rate of a UHMWPE cup coupled to a ZrO_2 head depends on the total protein concentration. The wear rate decreased in the order CS1 > BSS+1.5(A+G) > CS2 > BSS+A+G > BSS $\simeq$ 0. The elongated wear particles generated in BSS+A+G and BSS+1.5(A+G) suggested that the adhesive wear mechanism was active, although a different wear mechanism was responsible for the wear in bovine sera (CS1 and CS2).

Acknowledgments

This work was supported in part by Health and Labor Science Research Grants provided by the Ministry of Health, Labor and Welfare of Japan to the Japan Fine Ceramics Center.

References

1) Affatato S, Bersaglia G, Emiliani D, Foltran I, Taddei P, Reggiani M, Ferrieri P, Toni A. The performance of gamma-and EtO-sterilised UHMWPE acetabular cups tested under severe simulator conditions. Part 2: wear particle characteristics with isolation protocols. Biomaterials 2003;24: 4045-4055
2) Wang A, Schmidig G. Ceramic femoral heads prevent runaway wear for highly crosslinked polyethylene acetabular cups by third-body bone cement particles. Wear 2003;255:1057-1063
3) Bragdon CR, Jasty M, Muratoglu OK, O'Connor DO, Harris WH. Third-body wear of highly cross-linked polyethylene in a hip simulator. J Arthroplasty 2003;18:553-561
4) Liao YS, McKellop H, Lu Z, Campbell P, Benya P. The effect of frictional heating and forced cooling on the serum lubricant and wear of UHMW polyethylene cups against cobalt-chromium and zirconia balls. Biomaterials 2003;24:3047-3059
5) Clarke IC, Chan FW, Essner A, Good V, Kaddick C, Lappalainen R, Laurent M, Mckellop H, McGarry W, Schroeder D, Selenius M, Shen MC, Ueno M, Wang A, Yao J. Multi-laboratory simulator studies on effects of serum proteins on PTFE cup wear. Wear 2001;250:188-198
6) Chandrasekaran M, Wei LY, Venkateshwaran KK, Batchelor AW, Loh NL. Tribology of UHMWPE tested against a stainless steel counterface in unidirectional sliding in presence of model synovial fluids: part 1.Wear 1998;223:13-21
7) Gispert MP, Serro AP, Colaco R, Saramago B. Friction and wear mechanisms in hip prosthesis: Comparison of joint materials behavior in several lubricants. Wear 2006;260:149-158
8) Shanbhag AS, Bailey HO, Hwang DS, Cha CW, Eror NG, Rubash HE. Quantitative analysis of ultrahigh molecular weight polyethylene (UHMWPE) wear debris associated with total knee replacements. J Biomed Mater Res Appl Biomater 2000;53:100-110
9) Calonius O, Saikko V. Analysis of polyethylene particles produced in different wear conditions in vitro. Clinical Orthopaedics and related research 2002;399:219-230
10) Takadama H, Hashimoto M, Mizuno M. Artificial lubricant solution analogous to bovine serum as a test medium for wear characterization of artificial hip joint, Proceeding of 10th International Conference and Exihibition of the European Ceramic Society, Berlin,Germany, 2007;17-21 June
11) Elfick APD, Smith SL, Green SM, Unsworth A. The quantitative assessment of UHMWPE wear debris produced in hip simulator testing: the influence of head ma-

terial and roughness, motion and loading. Wear 2001;249:517-527
12) McMullin BT, Leung MY, Shanbhag AS, McNulty D, Mabrey JD, Agrawal CM. Correlating subjective and objective descriptors of ultra high molecular weight wear particles from total joint prostheses. Biomaterials 2006;27:752-757
13) Urano H, Fukuzaki S. Influence of anionic compounds on adsorption behavior of bovine serum albumin at oxide-water interfaces. J Ferm Bioeng 1997;83:261-266
14) Williams RL, Williams DF. The effect of albumin on the wettability of pure metal and metal surfaces. J. Colloid Interface Sci. 1988;126:596-603
15) Fukusaki S, Urano H, Nagata K. Adsorption of protein onto stainless-steel surfaces. J Ferm Bioeng 1995;80:6-11
16) Urano H, Fukusaki S. Conformation of adsorbed bovine serum albumin governing its desorption behavior at alumina/water interfaces. J Biosci Bioeng 2000;99:105-111
17) Haynes C, Norde W. Globular proteins at solid/liquid interfaces. Colloid Surf B: Biointerfaces. 1994;2:517-566
18) Norde W, Haynes C. Thermodynamics of protein adsorption, in: J. L. Brash, P. Wojciechowski (Eds), Interfacial Phenomena and Bioproducts, Marcel Dekker, New York, 1996, pp. 122-144
19) Malmsten M. Formation of adsorbed protein layers. J Colloid Interface Sci 1998;207: 186-199
20) Liao YS, McKellop H, Lu Z, Campbell P, Benya P. The effect of frictional heating and forced cooling on the serum lubricant and wear of UHMW polyethylene cups against cobalt-chromium and zirconia balls. Biomaterials. 2003;24:3047-3059
21) Mckellop HA, Campbell P, Park SH. The origin of submicron polyethylene wear debris in total hip arthroplasty. Clin Orthop Rel Res 1995;311:3-20
22) Cooper JR, Dowson D, Fisher J. The effect of transfer film and surface roughness on the wear of lubricated ultra-high molecular weight polyethylene. Clin Mater 1993;14: 295-302
23) Davidson JA. Characteristics of metal, ceramic total hip bearing surafces and their effect on long-term ultra-high molecular weight polyethylene wear. Clin Orthop Relat Res 1993;294:361-378
24) Fisher J, Chan KL, Hailey JL, Shaw D, Stone M. Preliminary study of the effect of aging following irradiation on the wear of ultrahigh-molecular-weight polyethylene. J Arthroplasty. 1995;10:689-692
25) Fisher J, Copper J, Dowson D, Isaac G, Wroblewski B. 1993. Wear mechanisms and sub-surface failure in UHMWPE acetabular cups. In: Proceedings of the 39th Annual Meeting of the Orthopaedic Research Society. USA, San Francisco, pp.509
26) Mcdonald MD, Bloebaum RD. Distinguishing wear and creep in clinically retrieved polyethylene inserts. J. Biomed Mater Res 1995;29:1-7
27) Campbell P, Dorey F, Amstutz AC. Wear and morphology of ultra-high-molecular-weight-polyethylene wear particles from total hip replacements. Proc Inst Mech Eng Part H. 1996;210:167-174
28) Pienkowski D, Jacob R, Hoglin D, Saum K, Kaufer H, Nicholls PJ. Low-voltage scanning electron microscopic imaging of ultra-high-molecular-weight polyethylene. J Biomed Mater Res. 1995;29:1167-1174

(Received: May 27/
Accepted: Jun 10)

Corresponding author:
Dr. Masami HASHIMOTO
Japan Fine Ceramics Center
2-4-1 Mutsuno, Atsuta-ku,
Nagoya, 456-8587 Japan
Tel. +81-52-871-3500
Fax +81-52-871-3599
E-mail: masami@jfcc.or.jp

Selection of highly osteogenic and chondrogenic cells from bone marrow stromal cells in biocompatible polymer-coated plates

G. Liu,[1,2] K. Iwata,[1,2] T. Ogasawara,[1,2] J. Watanabe,[3] K. Fukazawa,[3] K. Ishihara,[3,4] Y. Asawa,[1] Y. Fujihara,[1] U.-L. Chung,[4] T. Moro,[5] Y. Takatori,[2] T. Takato,[2] K. Nakamura,[2] H. Kawaguchi,[2] K. Hoshi[1]

[1]*Department of Cartilage and Bone Regeneration (Fujisoft), Graduate School of Medicine, The University of Tokyo, Tokyo, Japan*

[2]*Department of Sensory and Motor System Medicine, Graduate School of Medicine, The University of Tokyo, Tokyo, Japan*

[3]*Department of Materials Engineering, School of Engineering, The University of Tokyo, Tokyo, Japan*

[4]*Deparment of Bioengineering, School of Engineering, The University of Tokyo, Tokyo, Japan*

[5]*Center of Disease Biology and Integrative Medicine, Graduate School of Medicine, The University of Tokyo, Tokyo, Japan*

Received 4 September 2007; revised 31 October 2008; accepted 21 November 2008
Published online 27 March 2009 in Wiley InterScience (www.interscience.wiley.com). DOI: 10.1002/jbm.a.32460

Abstract: To enrich the subpopulation that preserves self-renewal and multipotentiality from conventionally prepared bone marrow stromal cells (MSCs), we attempted to use 2-methacryloyloxyethyl phosphorylcholine (MPC) polymer-coated plates that selected the MSCs with strong adhesion ability and evaluated the proliferation ability or osteogenic/chondrogenic potential of the MPC polymer-selected MSCs. The number of MSCs that were attached to the MPC polymer-coated plates decreased with an increase in the density of MPC unit (0–10%), whereas no significant difference in the proliferation ability was seen among these cells. The surface epitopes of CD29, CD44, CD105, and CD166, and not CD34 or CD45, were detectable in the cells of all MPC polymer-coated plates, implying that they belong to the MSC category. In the osteogenic and chondrogenic induction, the MSCs selected by the 2–5% MPC unit composition showed higher expression levels of osteoblastic and chondrocytic markers (COL1A1/ALP, or COL2A1/COL10A1/Sox9) at passage 2, compared with those of 0–1% or even 10% MPC unit composition, while the enhanced effects continued by passage 5. The selection based on the adequate cell adhesiveness by the MPC polymer-coated plates could improve the osteogenic and chondrogenic potential of MSCs, which would provide cell sources that can be used to treat the more severe and various bone/cartilage diseases. © 2009 Wiley Periodicals, Inc. J Biomed Mater Res 92A: 1273–1282, 2010

Key words: bone marrow stromal cell (MSC); 2-methacryloyloxyethyl phosphorylcholine (MPC) polymer; osteogenesis; chondrogenesis; cell adhesion

INTRODUCTION

Bone marrow mesenchymal stem cells or stromal cells (MSCs) retain the potential to differentiate into multiple cell lineages that include osteoblasts, chondrocytes, adipocytes, myoblasts, and early progenitors of neural cells.[1–3] Because MSCs can be easily obtained from a small aspirate of bone marrow and they rapidly proliferate during the early passages of the expansion culture, human MSCs are regarded as one of the attractive cell sources for regenerative medicine in bone, cartilage, heart, nerve, and other tissues. However, MSCs are principally collected from bone marrow aspirates only through their selection by adhesiveness onto the plastic culture dishes,[4] and therefore, they include various subpopulations of cells which possess different proliferation rates or differentiation potentials. During the long-term culture with repeated passages, the balance among the subpopulations in the MSCs changes as a result of the difference in the proliferation rates, which may cause a deterioration of the self-renewal property or multipotentiality after repeated passages.[5]

To isolate or enrich the subpopulation that preserves the self-renewal and the multipotentiality

Correspondence to: K. Hoshi; e-mail: pochi-tky@umin.net
Contract grant sponsor: Grants-in-Aid for Scientific Research from the Japanese Ministry of Education, Culture, Sports, Science and Technology, Japan; contract grant numbers: 18659593, 18592166

from the conventionally prepared MSCs, various kinds of efforts have been made in the past decade. It was reported that the sizes and structures of the cells could distinguish the cells possessing a great potential for multilineage differentiation, termed rapid self-renewal (RS) cells, from the heterogeneity of the MSCs.[6] The RS cells had a shaped round shape with approximately a 7-μm diameter, and could be purified by using a 10-μm filter.[6] However, some limitations had been pointed out in the paper that the filtration process could only provide a low yield of purified RS cells because the other-sized cells rapidly obstructed the filter pores. The RS cells were also characterized by the low forward scatter and low side scatter of light during a flow cytometric analysis.[7] During cell sorting with the criteria of a low forward scatter and low side scatter, the subpopulation was successfully enriched for the RS cells, which increased the differentiation potential for osteoblasts and adipocytes. Although the cell sorting technologies of flow cytometry have been highly anticipated for the effective isolation of a specific subpopulation, some issues including the acquisition rates of target cells, the prevention of pathogen contamination, or the mechanical and thermodynamic damage to cells by the cell sorter should be cautiously evaluated before clinical use.

The MSC isolation was also attempted, using some surface epitopes, including CD13, CD29 (integrin β1), CD44 (hyaluronan receptor), CD73(SH3), CD90 (Thy-1), CD105 (Endoglin), CD166 (activated leukocyte cell adhesion molecule/ALCAM), PDGF receptor or Stro-1, all of which are highly expressed in the MSCs.[6,8] The combination with CD34 and CD45 (leukocyte common antigen/LCA), either of which is a marker of hematopoietic stem cells, could exclude the hematopoietic lineage from the MSCs. However, as the expression level of the markers in the MSCs was quite similar to those of fibroblastic cells that are also contained in bone marrow aspirates and that decrease the multipotency and self-renewal,[8] specific selection of the MSCs from such heterogenetic cell populations could not be sufficiently obtained even by flow cytometry or a magnetic cell sorting system.

Serum deprivation is one of the possible methods to concentrate the subpopulation possessing a high proliferation and differentiation potential from the heterogeneity of the MSCs.[9] When early-passage human MSCs were cultured in serum-free medium without cytokines or other supplements, a subpopulation of the cells was attached to the plates and survived for 2–4 weeks. Afterward, such cells began to proliferate in serum-containing medium, and prominently showed stem cell properties including long telomeres or a high expression of the octomer-binding transcription factor 4 (OCT-4). The findings suggested that such cells that possess a strong adherent ability and survive despite the harsh environments may show a high quality of stem cell properties.

On the basis of this hypothesis, we attempted to select some subpopulations of MSCs showing a high adhesiveness on the culture plates. For selection, the cell adhesiveness was adjusted by the coating of 2-methacryloyloxyethyl phosphorylcholine (MPC) polymers. The MPC polymers are designed with inspiration from cell membrane surface and well-known biocompatible polymers that can reduce protein adsorption or subsequent cell adhesion significantly.[10–12] On the basis of this fundamental biocompatibility, the MPC polymers have been used for preparing medical devices, for example, the surfaces of intravascular stents, intravascular guide wires, soft contact lenses, an artificial lung or artificial hip joint.[13–16] Some of these are already clinically available.

We examined the selectivity of MSCs using MPC polymer-coated plates and evaluated the proliferation ability or differentiation potential of the MPC polymer-selected subpopulation. Especially, we focused on the osteogenic and chondrogenic ability, because bone and cartilage tissue engineering using MSCs are highly desired for clinical applications.

MATERIALS AND METHODS

Preparation of MPC polymer-coated plates

Coating of the MPC polymer onto the polystyrene (PS) surface of the culture plates was performed by a simple dip-coating using MPC polymer solutions. The composition of MPC units was controlled by mixing poly(*n*-butyl methacrylate) (Poly(BMA)) and poly(MPC-*co*-BMA)(PMB30). These polymers were synthesized by a conventional radical polymerization. Poly(BMA) was a homopolymer of BMA without MPC unit (molecular weight = 4.0×10^5), and PMB30 was a copolymer composed of 30% of MPC units and 70% of BMA units (molecular weight = 6.0×10^5). In this study, each polymer was dissolved in a mixture of tetrahydrofran (THF) and ethanol (1:9 by volume) as solvents, and then poly(BMA) and PMB30 solutions were prepared (0.25 wt %). To control the MPC unit composition in the range between 0, 1, 2, 5, and 10% of MPC unit composition, these polymer mixtures in the solution were prepared. The dip-coating was carried out in the clean bench as follows: (i) 200 μL of the solution was poured into the each culture plates (ϕ 2.2 cm), (ii) the polymer solution was removed after 5 s, (iii) the coating was repeated and the resulting culture plate was dried over night, and (iv) the MPC polymer-coated culture plate was sterilized by UV irradiation for an adequate time. Therefore, the resulting MPC unit density on the plate was 0, 1, 2, 5, and 10% MPC unit composition.

Surface elemental analysis of the MPC polymer-coated PS plate was carried out by X-ray photoelectron spectroscopy (XPS, AXIS-His, Shimadzu/KRATOS, Kyoto, Japan). The X-ray source used for XPS measurements was Mg Ka source. The take-off angle of the photoelectrons was fixed

as 90°. At least five points of the sample were measured by XPS and these intensities were averaged before the following calculation. The surface compositions of the MPC units were calculated as follows. The ratio of signal intensity at 133 eV based on the phosphorus atom attributed to the MPC units over that at 285 eV based on the carbon atoms attributed methyl groups and methylene groups in both BMA and MPC units was determined. The calibration was carried out using the ratio obtained from the XPS spectra of both poly(BMA) and poly(MPC)-coated PS plate as 0% and 100% of MPC unit, respectively.

MSC preparation and selection by MPC polymer-coated plates

All procedures for the present experiments were approved by the ethics committee or institutional committee for animal research of the University of Tokyo Hospital (ethics permission #622). Figure 1(a) indicates the experimental design. Human MSCs were obtained from the femur of osteoarthritic patients who underwent total hip replacement at the University of Tokyo Hospital, after informed consent. Cells in bone marrow aspirates (100 μL/φ 2.2 cm dish) were seeded on MPC polymer-coated culture plates with various MPC unit compositions as 0–10%, and cultured using the hMSC bullet kit (Cambrex, East Ruatherford, NJ) in a 37°C/5% CO_2 incubator. Rat MSCs were collected from 6-week-old male Sprague-Dawley rats (Nisseizai, Tokyo, Japan). After the epiphyses of the tibias were removed, the marrow was flushed out by using a syringe filled with medium and filtered through a 70-μm nylon mesh. The obtained bone marrow materials (100 μL/φ 2.2 cm dish) were plated and cultured in the same manner as human MSCs.

The cells were harvested by treatment using trypsin-EDTA solution. After the cell harvest of the primary culture from the MPC polymer-coated plates, the cells were reseeded onto the conventional PS culture plates at a density of 5.0×10^3 cells/cm^2. Passages were performed when the cells were approaching confluence. The medium was changed three times per week. The cell numbers were counted by a haematocytometer, while the viability of the cells was checked by trypan blue staining. Cell proliferation was also colorimetrically measured by cell counting kit-8 (Dojin, Kumamoto, Japan), a week after cell seeding.

Flow cytometric analysis

Cells were harvested using trypsin-EDTA solution, centrifuged at 1500*g* for 5 min, and resuspended at 5×10^6 cells/mL in phosphate-buffered saline (PBS) containing 3% fetal bovine serum. Aliquots containing 10^5 cells were incubated with individual primary antibodies or control IgG for 30 min at room temperature. The cells were washed in PBS containing 3% fetal bovine serum and incubated with a fluorescent conjugated secondary antibody for 30 min at room temperature. Samples were analyzed using a FACS LSL II (BD, Franklin Lakes, NJ). The following monoclonal antibodies were used: mouse monoclonal antibodies against human CD29 (integrin β1, BD), human CD34 (Chemicon, Victoria, Australia), human CD44 (hyaluronan receptor, Ancell, Bayport, MN), human CD45 (LCA, Cymbus, Chandlers Ford, UK), human CD105 (Endoglin, Ancell), CD166 (ALCAM, Ancell), normal mouse IgG (Santa Cruz Biotechnology, Santa Cruz, CA) and fluorescein isothiocyanate (FITC)-conjugated rabbit antibody against mouse IgG (Santa Cruz Biotechnology).

Osteogenic and chondrogenic induction for MSCs

The osteogenic[1] or chondrogenic[17,18] differentiation was induced in MSCs according to previously reported procedures with some modifications. For the osteogenic differentiation, cells were seeded at 4.0×10^4 cells per 2.2-cm plates and maintained for 21 days in DMEM supplemented with 10% fetal bovine serum, 10 m*M* β-glycerophosphate, 100 n*M* Dexamethasone, and 50 μg/mL ascorbic acid-2-phosphate. For the chondrogenic differentiation, cells were seeded at 2×10^5 cells per 15 mL plastic centrifuge tube and maintained in 2 mL of serum-free a-MEM supplemented with 3500 μg/mL glucose, 6.25 μg/mL insulin, 6.25 μg/mL transferrin, 6.25 ng/mL selenite, 5.33 μg/mL linolate, 1.25 mg/mL bovine serum albumin, 10 ng/mL transforming growth factor-β3, 100 n*M* dexamethasone and 50 μg/mL ascorbic acid-2-phosphate. The cells were cultured under the chondrogenic status for 21 days. The medium was changed three times per week.

Total RNA extraction and real-time RT-PCR

The total RNA was isolated from MSC using the chaotropic Trizol method (Nippon-gene, Tokyo, Japan). The total mRNA (1 μg) was reverse transcribed using the Super Script reverse transcriptase with a random hexamer (Takara Shuzo, Shiga, Japan). The full-length or partial-length cDNA of the target genes, including the PCR amplicon sequences, was amplified by PCR, cloned into pCR-TOPO Zero II or pCR-TOPO II vectors (Invitrogen, Carlsbad, CA), and used as standard templates after linearization. The QuantiTect SYBR Green PCR Master Mix (Qiagen, Hilden, Germany) was used, and the SYBR Green PCR amplification and real-time fluorescence detection were performed with an ABI 7700 Sequence Detection system (Foster City, CA). All reactions were run in quadruplicate. The sequences of the primers were 5′-CTCCT CGCTTTCCTTCCTCT-3′ and 5′-GTGCTAAAGGTGCCAA TGGT-3′ for COL1A1; 5′-GAGTCAAGGGTGATCGTGGT-3′ and 5′-CACCTTGGTCT CCAGAAGGA-3′ for COL2A1; 5′-AGGAATGCCT GTGTCTGCT T -3′ and 5′-ACAGGCC TACCCAAACATGA-3′ for COL10A1; 5′- GACCCTTGACC CCCACAAT-3′ and 5′- GCTCGTACTGCATGTCCCCT-3′ for ALP; 5′-CATG AGCGAGGG CACTCC-3′ and 5′-TCGCTTCAGGTCAGCCTTG-3′ for Sox9; 5′-GAAGGTGA AGGTCGGAGTCA-3′ and 5′-GAAGATGGTGATGGGAT TTC-3′ for GAPDH.

Enzyme activity for ALP

The enzyme activity was histochemically detected in the MSCs in which the osteogenic differentiation was induced.

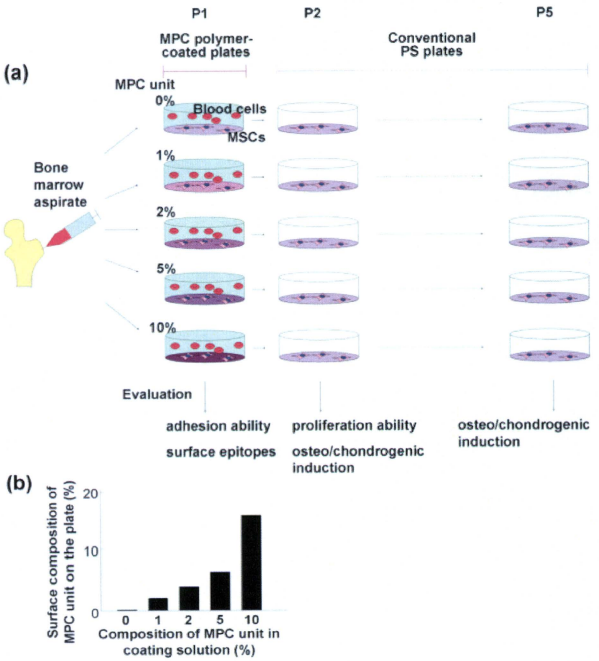

Figure 1. (a) The experimental design. Cells in bone marrow aspirates were seeded on MPC polymer-coated plates at the composition of 0–10% MPC unit, at passage 1, while the adhesion ability of MSCs to the MPC polymer-coated plates and the surface epitopes of MPC-selected cells were evaluated. Although cells were cultured on the MPC polymer-coated plates at passage 1, the cells were seeded onto the conventional PS plates thereafter. The proliferation of cells (passage 2) was measured by cell counting, while the differentiation potential for osteogenesis and chondrogenesis was examined at passages 2 and 5. (b) Relationship between MPC unit composition at the surface on PS plate after coating and that in polymer-coating solution. [Color figure can be viewed in the online issue, which is available at www.interscience.wiley.com.]

For ALP enzyme histochemistry, the cells were incubated with a mixture of 5 mg naphthol AS-BI phosphate (Sigma, St. Louis, MO) as a substrate and 18 mg of fast red violet LB salt (Sigma) diluted in 30 mL of 0.1 mol/L Tris-HCl buffer (pH 8.5). The images were taken by the digital camera, while the enzyme activity was quantitatively measured by histomorphometrical approaches using the software Scion Image alpha 4.0.3.2 (Scion, Frederick, MD).

RESULTS

Selection using MPC polymer-coated plates

Polymer coating of PS culture plate with the PMB30/poly(BMA) mixed solution was proceeded well, and the surface of the plate was covered with these polymers, completely. When the surface composition of MPC units on the plates was calculated from the XPS results, it was found that the MPC unit composition at the surface increased in parallel with that in the polymer mixed solution containing poly(BMA) and PMB30 used in a single dip coating as shown in Figure 1(b). We confirmed that the surface composition the MPC units could be controlled.

With these plates, we first selected some subpopulations of the MSCs according to the degrees of the adhesiveness on the culture plates coated with different compositions of the MPC unit. Human bone marrow aspirates (~0.1 mL) was seeded onto the culture plates with a 2.2 cm diameter coated with 0, 1, 2, 5, and 10%